AGU PUBLICATIONS

Geophysical Research Letters

RESEARCH LETTER
10.1002/2013GL059164

Key Points:
- Coupling of plasma and neutral gas dynamics in sprites
- Mechanism of infrasound radiation from sprites
- Dependence of infrasound amplitudes on sprite currents

Correspondence to:
C. L. da Silva,
caitano.dasilva@psu.edu

Citation:
da Silva, C. L., and V. P. Pasko (2014), Infrasonic acoustic waves generated by fast air heating in sprite cores, *Geophys. Res. Lett.*, *41*, 1789–1795, doi:10.1002/2013GL059164.

Received 27 DEC 2013
Accepted 10 FEB 2014
Accepted article online 14 FEB 2014
Published online 7 MAR 2014

Infrasonic acoustic waves generated by fast air heating in sprite cores

Caitano L. da Silva[1] and Victor P. Pasko[1]

[1]CSSL Laboratory, Pennsylvania State University, University Park, Pennsylvania, USA

Abstract Acceleration, expansion, and branching of sprite streamers can lead to concentration of high electrical currents in regions of space, that are observed in the form of bright sprite cores. Driven by this electrical current, a series of chemical processes take place in the sprite plasma. Excitation, followed by quenching of excited electronic states leads to energy transfer from charged to neutral species. The consequence is heating and expansion of air leading to emission of infrasonic acoustic waves. Results indicate that $\gtrsim$0.01 Pa pressure perturbations on the ground, observed in association with sprites, can only be produced by exceptionally strong currents in sprite cores, exceeding 2 kA.

1. Introduction

Sprites are large-scale electrical discharges occurring between 40 and 90 km altitude [*Sentman et al.*, 1995]. They are generated by strong quasi-electrostatic fields produced by cloud-to-ground lightning discharges in an underlying thunderstorm. Sprites have been extensively studied through measurements of their optical emissions [e.g., *Stenbaek-Nielsen and McHarg*, 2008] and remote sensing of their electromagnetic fields [e.g., *Cummer et al.*, 1998]. In recent years, a new possibility for sprite remote sensing has been realized: infrasound signatures recorded on the ground have been unambiguously associated with sprites [*Farges et al.*, 2005]. The possibility of infrasound generation by sprites was first proposed by *Bedard et al.* [1999]. *Liszka* [2004] reported the detection of infrasound signatures that were associated with sources at mesospheric altitudes during times of intense thunderstorm activity. These findings were confirmed by *Farges et al.* [2005], whose authors have correlated the infrasound recordings (in the frequency range of 0.1–9 Hz) with optical sprite observations. Typical sprite infrasound amplitudes are 0.01–0.1 Pa, as measured on the ground, at distances ~100–400 km from the source [*Farges et al.*, 2005; *Farges and Blanc*, 2010]. Long-range sprite infrasound signatures have a chirp-like feature, with low frequencies arriving at the detector before high frequencies [*Farges et al.*, 2005].

Analysis of energy budget in sprites, based on optical emissions, indicate that on average several to tens of MJ are deposited in the atmosphere per sprite event [e.g., *Sentman et al.*, 2003; *Kuo et al.*, 2008]. *Pasko and Snively* [2007] demonstrated that an energy deposition of hundreds of MJ in sprites is necessary to produce infrasound amplitudes ~0.1 Pa as measured on the ground, far away from the source. Further modeling studies of infrasound propagation in a realistic atmosphere with frequency- and altitude-dependent attenuation of acoustic waves were undertaken by *de Larquier* [2010] and *de Larquier and Pasko* [2010]. *de Larquier* [2010, pp. 51–56] demonstrated that a local pressure modification of 1%, occurring within a cylindrical source of 1.5 km radius and 5 km height centered at 75 km altitude, is capable of producing infrasound amplitudes of $\sim 10^{-3}$ Pa, as measured by an observer at the ground ~400 km away from the source. Modeling results by *Pasko and Snively* [2007] and *de Larquier* [2010, pp. 51–56] support the ideas advanced by *Farges et al.* [2005] that the long-range chirp-shape signature can be explained by the horizontal size of the whole sprite. The infrasound signal coming from the nearest side of the sprite (relatively to the sensor) reflects at higher altitude, has reduced high-frequency content due to strong absorption at high altitudes, and arrives first at the observation point. The infrasound signal generated from the farthest side of the sprite reflects at lower altitude, has enhanced high-frequency content, and arrives second at the observation point.

In this letter we describe the mechanism of infrasonic acoustic wave generation by fast air heating in sprite cores, and the relationship between infrasound amplitudes and sprite currents. This work is the first step toward connecting optical [e.g., *Stenbaek-Nielsen and McHarg*, 2008] and electromagnetic [e.g., *Cummer et al.*, 1998] properties of sprites, with their acoustic signatures [e.g., *Farges et al.*, 2005].

2. Model Formulation

The models employed to study the sprite development, and their effects in the mesosphere, can be divided in two groups: (1) models of individual sprite streamer channels developing under externally applied lightning electric field [e.g., *Liu et al.*, 2009; *Luque and Ebert*, 2010; *Qin et al.*, 2013], and (2) models of in situ chemical effects of sprite electric fields [e.g., *Sentman et al.*, 2008; *Gordillo-Vazquez*, 2008; *Gordillo-Vazquez and Luque*, 2010]. The first group of models is successful in explaining the dynamics of individual streamers, specially of their optical emissions. Their drawback is that they can only simulate time scales shorter than a few milliseconds, mainly because on longer time scales streamers branch and cannot be fully described by an axisymmetric 2-D fluid model. The second group of models simulate a control volume in the mesosphere subjected to the passage of a sprite streamer. They account for an extensive list of chemical processes taking place in the sprite plasma on time scales of up to hundreds of seconds after the sprite occurrence. The drawback of these models is the usage of a 0-D geometry, not accounting for axial and radial dynamics in sprite channels. In order to investigate the levels of air heating within sprites and the mechanism of infrasound generation, we have developed a new model that describes the coupling between charged and neutral species in the sprite plasma that leads to ambient gas heating. The model is implemented in a 1-D (radial) geometry and accounts for over 100 chemical reactions, providing a synergistic connection between the two above mentioned classes of models, i.e., between spatial dynamics and composition of the sprite plasma.

The conceptual model of the sprite infrasonic source is depicted in Figure 1a. Sprites manifest themselves in the form of streamer discharges or, more precisely, streamer coronas. Typically, a sprite is initiated from a local inhomogeneity present in the lower ionospheric conductivity, developing as an initial downward positive streamer that accelerates, expands, and branches [e.g., *Liu et al.*, 2009]. In some sprites, the development of downward streamers is followed by the formation of upward streamers, depending on the available lightning electric field [*Qin et al.*, 2013]. Sprites with only downward streamers are referred to as column sprites, while those with both downward and upward streamers are referred to as carrot sprites. A common characteristic for both types of morphologies is the existence of a bright core associated with the path traced by the first downward streamer. The schematics of a sprite core, shown in Figure 1a, is consistent with sprite morphology observed at submillisecond time resolution [*Cummer et al.*, 2006]. We associate the strong brightness of the sprite core, as evidenced in high-speed imagery [e.g., *Cummer et al.*, 2006; *Stenbaek-Nielsen and McHarg*, 2008], with the passage of a strong current through it. This mechanism is different from the one associated with processes in the sprite streamer heads, where very bright and compact regions are formed due to the existence of strong space charge fields of ~ 3–$5E_k$ [e.g., *Liu et al.*, 2009] (where E_k is the breakdown threshold field defined by the equality between ionization and two-body attachment frequencies in air [e.g., *Raizer*, 1991, p. 135]). As inferred from optical observations [e.g., *Cummer et al.*, 2006], the sprite core has a length $L_z \simeq 10$ km. On the other hand, the transverse scale L_r is of the order of tens to hundreds of meters. Since $L_z \gg L_r$, we represent the sprite core by a 1-D axisymmetric radial system, located at an altitude $h = 70$ km, as schematically shown in Figure 1a.

In this conceptual model the sprite current I_{sprite}, as inferred from remote sensing of electromagnetic fields [e.g., *Cummer et al.*, 1998], is not flowing in the whole cross-sectional area of a sprite (~ 1000 km^2), but it is rather confined within the several sprite cores, which have substantially higher conductivity than the regions of the atmosphere in their vicinity. The number of sprite cores N_{core} can vary from event to event, typically from a few to tens of cores, and for quantitative analysis conducted in this paper, we assume that on average a sprite has $N_{\text{core}} = 10$. The current flowing through a given sprite core, therefore, is $I_{\text{core}} = I_{\text{sprite}}/N_{\text{core}}$. The inset in Figure 1a shows the $I_{\text{core}}(t)$ waveform adopted in our simulations. The waveform is characterized by three parameters: the peak current I_p, the rise time τ_p (to rise the current from the initial value I_0 to its peak I_p), and the duration of the strong current phase $\Delta\tau_I$. We assume that the peak current is sustained during the time interval $\tau_p \leq t \leq \tau_p + \Delta\tau_I$. For $t > \tau_p + \Delta\tau_I$ the current slowly decreases as $\propto 1/t$ [e.g., *Barrington-Leigh et al.*, 2002]. The maximum current flowing through a sprite can be estimated from a moving capacitor plate model [e.g., *Pasko et al.*, 1998; *Barrington-Leigh et al.*, 2002] as being $\sim I_Q h_Q/h_{\text{I}}$, where I_Q is the current of the parent cloud-to-ground lightning, h_Q is the altitude of charge removal from the thundercloud, and h_{I} is the lower ionospheric altitude, or the altitude of the moving capacitor plate. For a lightning with high peak current ~ 100 kA, and $h_Q/h_{\text{I}} \simeq 1/5$ (e.g., $h_Q = 10$ km and $h_{\text{I}} = 50$ km), one gets $I_{\text{sprite}} \leq 20$ kA. We note that, although rare, sprite currents of ~ 20 kA were already observed [e.g., *Hager et al.*, 2012]. Complementarily, *Cummer et al.* [1998] measured peak currents $I_{\text{sprite}} \simeq 2$ kA. Therefore, we estimate

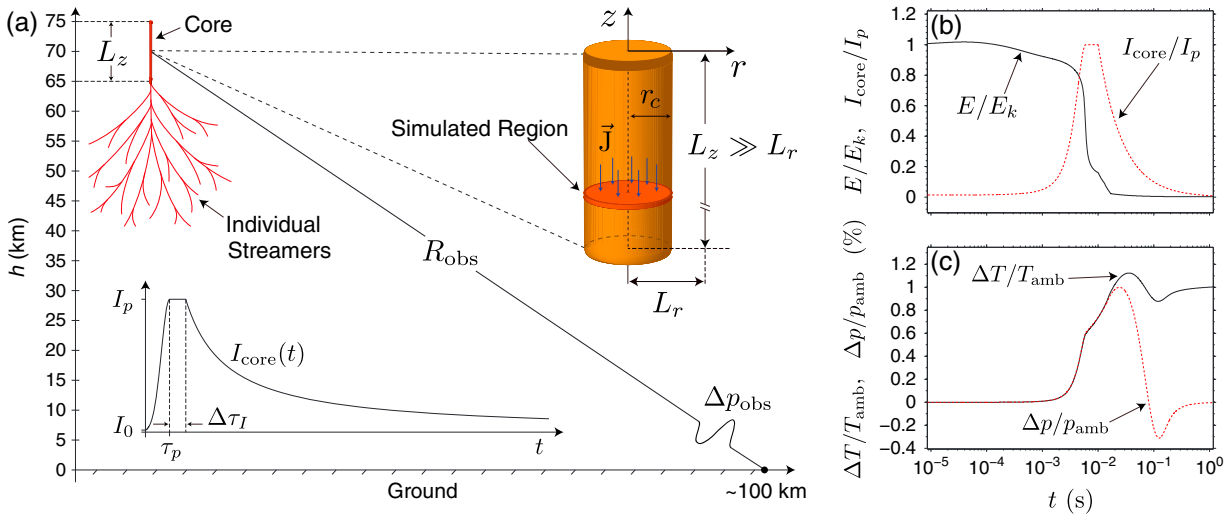

Figure 1. (a) Schematics of air heating in a sprite core leading to generation of infrasonic acoustic waves observed on the ground, at a distance R_{obs} from the source. The figure highlights the geometry of the simulated region, which describes a cross section of the sprite core at $h = 70$ km altitude. The inset shows the waveform of the current flowing through the sprite core, $I_{core}(t)$. (b) Time dynamics of electric field and current, and (c) maximum modification in temperature and pressure.

that realistic peak currents I_p in bright sprite cores should range between 200 and 2000 A. The time scales τ_p and $\Delta\tau_I$ are adjusted to make the waveform shown in Figure 1a resemble the measurements.

To describe the physical/chemical processes in the sprite core plasma, we have developed a model consisting of four main blocks: (1) a set of nonlinear neutral gas dynamics equations; (2) a detailed kinetic scheme accounting for the most important processes in a gas discharge plasma; (3) energy exchange between charged and neutral particles accounting for the partitioning of the electronic power between elastic collisions, excitation of vibrations, and excitation of electronic states; and (4) delayed vibrational energy relaxation of nitrogen molecules [*da Silva and Pasko*, 2013a]. This model has also been applied to simulation of leader speeds at reduced air densities and for interpretation of the phenomenology of gigantic jets [*da Silva and Pasko*, 2012, 2013b]. An important feature of this model is the capability of calculating the fraction of discharge power σE^2 (where σ is electrical conductivity and E electric field) that is directly used for heating of air in the so called "fast heating" mechanism [e.g., *Popov*, 2011] and its dependence on ambient air density N_{amb}. The fast heating mechanism accounts for quenching of excited electronics states, electron impact dissociation, and electron-ion recombination [*da Silva and Pasko*, 2013a, Sections 2.3 and 3.2].

The initial conditions for the simulation are set to make the sprite core resemble a single sprite streamer channel at 70 km altitude (right after the passage of the first streamer head), i.e., the electron density has a Gaussian radial distribution $n_e = n_{e,a} e^{-r^2/r_c^2}$, where $n_{e,a} = 10^6$ cm^{-3} and $r_c = 20$ m. Charge neutrality is ensured by setting $n_{O_2^+} = n_e$, where $n_{O_2^+}$ is the density of O_2^+ ions. The value $n_{e,a}$ is the typical electron density in a streamer body as obtained from sprite streamer simulations [e.g., *Liu et al.*, 2009], while r_c is consistent with high-speed optical observations of initial sprite streamer radii [*Kanmae et al.*, 2012]. The choice for r_c is also consistent with observed acoustic spectral content, i.e., a cylindrical acoustic radiator with a diameter of 40 m is expected to produce dominant frequencies below $c_s/2r_c \simeq 8$ Hz, where c_s is the ambient speed of sound. The initial condition for the electric current is $I_0 = q_e(\mu_e + \mu_p) n_{e,a} E_k \pi r_c^2 \simeq 26$ A, where q_e is the electronic charge, and μ_e and μ_p are the mobilities of electrons and positive ions, respectively. The ambient temperature and pressure at 70 km altitude are $T_{amb} = 200$ K and $p_{amb} = 4.68$ Pa, respectively. We apply the current I_{core} to the cross sectional area of the sprite core, and we track the plasma parameters, i.e., densities of charged and neutral particles, electric field, translational and vibrational temperature of neutrals, air pressure, etc., as a function of time t, and radial position r, in a cylindrical domain of size $L_r = 400$ m.

3. Results

The input parameter of the model is the current flowing in the sprite core I_{core}. To illustrate the mechanism of infrasonic acoustic wave generation in the sprite core by fast air heating we first show a reference case. We chose a peak current $I_p = 2000$ A in the upper range of sprite core currents (discussed in the previous

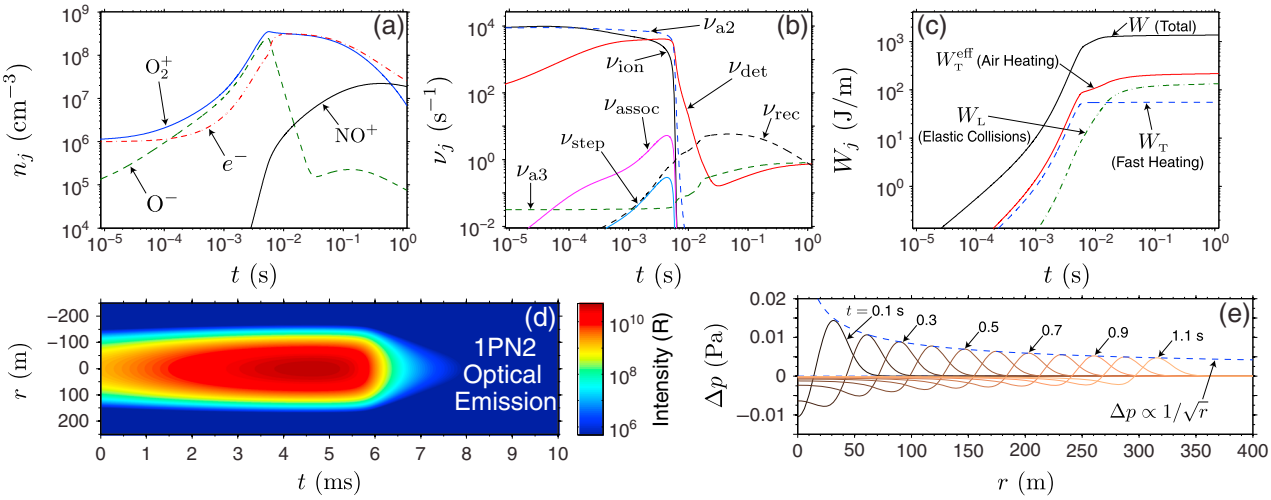

Figure 2. (a and b) Time dynamics (at the axis of symmetry) of main charged species, and effective frequencies of electron production and loss. (c) Energy deposited per unit channel length. (d) Optical emissions. (e) Radial expansion of pressure wave.

section), to emphasize that only extraordinary sprites can produce infrasound signatures detectable on the ground. The other parameters of the current waveform are $\tau_p = 6$ ms and $\Delta\tau_f = 4$ ms. Results are shown in Figures 1b–1c and 2a–2e. Figure 1b shows the applied current and the calculated electric field from Ohm's law, it can be seen that an electric field plateau of $\sim E_k$ is sustained during the current growth phase. Figure 1c shows the percent change in temperature and pressure at the axis of symmetry of the sprite core. It can be seen that the maximum modification in pressure is ~1% and that the highest rate of pressure growth occurs during the current rise stage. Figures 2a–2b show the time dynamics of main charged species and effective frequencies of electron production and loss, following nomenclature used by *da Silva and Pasko* [2013a, Section 2.2 and Table A1]. Ohm's law indicates that the increase in current should drive an increase in the electric field; however, an incremental increase in the electric field above E_k leads to increase in ionization (ν_{ion}) that leads to conductivity enhancement and reduction of the electric field. Hence, the above mentioned plateau $E \approx E_k$ is formed. In these conditions two-body attachment (ν_{a2}) and ionization rates balance each other. Figures 2a–2b show that the resulting increase in electron density in the sprite core is resulting from the accumulation of O^- ions followed by electron detachment (ν_{det}), in agreement with conclusions of more detailed kinetic models [*Gordillo-Vazquez and Luque*, 2010]. On longer time scales ($t \gtrsim 1$ s), the plasma decays owing to electron-ion recombination (ν_{rec}) and three-body attachment (ν_{a3}). The above described mechanism for the quick establishment of $E \approx E_k$ makes our modeling results independent of the initial electric field in the sprite core. If initially $E < E_k$, the field will rapidly grow to a value near E_k.

Figure 2c shows the energy deposited in the sprite core per unit of channel length $W(t)$ (which is obtained by integrating σE^2 over the cross-sectional area of the sprite core and in time, i.e., $W(t) = \int_0^t IE(t')dt'$). Total energy deposited per unit channel length is $W = 1.37$ kJ/m (see Figure 2c at the end of the simulation, i.e., $t \simeq 1$ s), which translates in a total energy deposited in the sprite $N_{core}L_z W = 137$ MJ. Figure 2c also shows the calculated amount of energy transferred to heating of air $W_T^{eff}(t)$, including fast heating, elastic collisions, heating from ion current, and vibrational-translational energy relaxation (W_T^{eff} is obtained by integration of the effective heating rate Q_T^{eff}, following nomenclature used by *da Silva and Pasko* [2013a, Section 2.3]). A total amount $W_T^{eff} = 217$ J/m is used for heating of air, which corresponds to only ~16 % of the total deposited energy. The two major channels for heating of air W_T^{eff} are also shown in Figure 2c. During the current rise stage, the fast heating mechanism, $W_T(t)$, is dominant. During latter stages, when electric field is signficantly below E_k, $W_L(t)$ is dominant; W_L accounts for energy transfer in elastic collisions, as well as excitation of rotations in O_2 and N_2, and vibrations in O_2. Comparing Figures 1b, 1c, and 2c, we can assert that the dominant contribution for pressure increase comes from the fast heating W_T, during the current rise stage. Moreover, calculation of optical emissions from the sprite core shows that the current rise is also associated with the maximum brightness of the sprite, as shown in Figure 2d. The sustained luminosity associated with rapid current growth is in agreement with the mechanism for the sprite streamer luminous

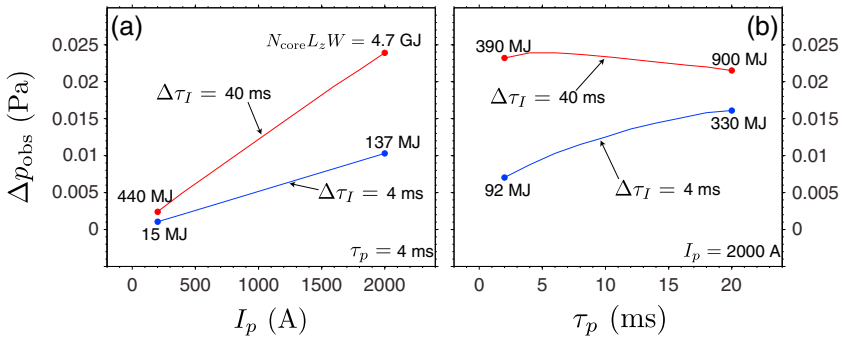

Figure 3. Estimated amplitude of infrasound measured at the ground Δp_{obs} as a function of the current waveform parameters. The horizontal distance between the sprite and the observation point is ~100 km, as depicted in Figure 1a. The circles at the end of the curves are eight sample cases for which the total deposited energy is also displayed.

trail proposed by *Liu* [2010]. The direct correlation between current waveform and sprite brightness is also evident in measurements [e.g., *Cummer et al.*, 1998, Figures 4–6].

Figure 2e shows the radial expansion of the pressure pulse. It can be seen that the response of the neutral gas to this weak source is approximately linear, i.e., pressure amplitudes decrease with distance as $\Delta p \propto 1/\sqrt{r}$, as highlighted by the dashed line in Figure 2e. The maximum pressure amplitude at a reference point $r_{ref} = 10\, r_c$ is $\Delta p_{ref} = 6 \times 10^{-3}$ Pa. We next estimate the infrasound amplitudes Δp_{obs} as measured by an observer on the ground far away from the source, from simple scaling derived from energy conservation. It can be demonstrated that the intensity of an acoustic wave $\mathcal{I}_s$ (expressed in units of J/m^2·s) is related to the amplitude of pressure perturbation as $\mathcal{I}_s = (\Delta p)^2/2\rho_{amb}c_s$ [e.g., *Blackstock*, 2000, pp. 48–51], where $\rho_{amb} = m_{air}N_{amb}$ is the ambient air mass density. Neglecting the effects of atmospheric absorption, the power generated by the source is conserved after the wave has propagated for a distance r, i.e., $\int_S \mathcal{I}_s dS =$ const, where the energy flux is integrated through a reference surface S surrounding the source. The area of this surface is $2\pi r L_z$ and $4\pi r^2$, for a long (cylindrical) radiator and for a (spherical) point source, respectively. Hence, the scaling of the pressure amplitudes with distance and altitude are approximately $\propto \sqrt{N_{amb}}/\sqrt{r}$ and $\propto \sqrt{N_{amb}}/r$, for cylindrical and spherical sources, respectively. Assuming that for sprites the cylindrical dependence holds for a distance about the vertical size of the acoustic radiator (i.e., L_z), we obtain:

$$\Delta p_{obs} = \Delta p_{ref} \sqrt{\frac{N_0}{N_{amb}}} \sqrt{\frac{r_{ref}}{L_z}} \left(\frac{L_z}{R_{obs}} \right), \tag{1}$$

where N_0 and N_{amb} are the ambient air densities at ground level and 70 km altitude, respectively. Assuming that the observation point is at a distance $R_{obs} = 100$ km from the source, as schematically shown in Figure 1a, and for the above defined length scales, this approach gives a correcting factor $\Delta p_{obs}/\Delta p_{ref} \simeq 1.72$, to estimate amplitudes on the ground from amplitudes at a reference position near the source. For the reference case, shown in Figures 1b–1c and 2a–2e, we have $\Delta p_{obs} = 0.01$ Pa, which is in the lower range of amplitudes reported in literature [*Farges et al.*, 2005; *Farges and Blanc*, 2010].

Formula (1) is a simple estimate of pressure amplitudes on the ground assuming that geometrical energy spreading is dominant over atmospheric absorption. It also neglects any interaction between coherent sources. For distances larger than ~100 km, the typical height of the Earth-Thermosphere waveguide, the scaling with distance is once again cylindrical, i.e., $\propto 1/\sqrt{r}$. This factor diminishes the pressure amplitude by only a factor of 2 as the wave propagates from 100 to 400 km. Although simple, formula (1) agrees with large-scale infrasound propagation models [*Pasko and Snively*, 2007; *de Larquier*, 2010], in the sense that a local modification of 1% in pressure leads to amplitudes of $\gtrsim$0.01 Pa measured on the ground.

Figures 3a–3b show the dependence of the pressure amplitude measured on the ground, estimated from formula (1), on the current waveform parameters. The total energy deposited in the sprite is also shown for eight cases (extremity of curves) for reference. It can be seen that Δp_{obs} is directly proportional to peak current. For instance, Figure 3a shows that a tenfold increase in I_p leads to an increase in Δp_{obs} of ~10, while a tenfold increase in $\Delta\tau_I$ leads only to doubling of Δp_{obs}. From Figure 3b, we can see that a tenfold increase in τ_p also introduces small changes in Δp_{obs}. On the other hand, the deposited energy in the sprite, $N_{core}L_zW$, increases proportionally to all three current waveform parameters. These results show that sprite infrasound

amplitudes measured at the ground are a better tracer of peak currents in sprites rather than total energy deposited and that a special care should be taken when estimating energy deposited in sprites from infrasound measurements. Only in the case when τ_p and $\Delta\tau_l$ are known quantities, the infrasound amplitudes uniquely translate into peak current and, consequently, in total deposited energy. Note that long time scales τ_p and $\Delta\tau_l$ are unrealistic. Under sprite conditions, they are expected to be of the order of a few milliseconds. However, we have included extreme cases in Figures 3a–3b to demonstrate that they weakly affect the pressure amplitudes.

4. Discussion

As demonstrated in previous section, significantly strong currents are required to produce the registered infrasound amplitudes at ground level $\gtrsim$0.01 Pa. We note also that individual streamer channels cannot produce any significant air heating at sprite altitudes. Assuming that the current in an individual streamer channel can be as low as a fraction of ampere, it indicates that hundreds to thousands of streamers have to be attached to a common stem, the sprite core, to produce observable acoustic radiation on the ground. Hence, not all sprites can produce detectable acoustic radiation. Nonetheless, we emphasize that air heating is the most likely mechanism for production of infrasonic acoustic radiation from sprites, as discussed below.

At near-ground-level pressure, corona discharges are known to produce sound [e.g., *Bastien*, 1987, Section 5]. A well-known example is the crackling and hissing noise produced by high-voltage transmission lines [e.g., *Straumann*, 2011, and references therein]. In these regimes two physical mechanisms determine the amplitude and spectrum of the generated acoustic radiation: momentum and energy transfer [e.g., *Bastien*, 1987, Section 2]. The former mechanism has been extensively studied in recent years in the context of air flow control by plasma actuators [e.g., *Roth*, 2003; *Boeuf et al.*, 2007] and it is associated with the electrohydrodynamic force $\rho_c\vec{E}$ (per unit volume) exerted by the plasma on the neutral gas, where ρ_c is the electrical charge density. The latter is the mechanism responsible for the formation of thunder in lightning [e.g., *Few*, 1986], where energy is transferred from the charged to neutral particles, at a rate σE^2 (per unit time and unit volume), in the discharge channel leading to Ohmic heating of air and expansion. In the case of sprites, the air heating/energy transfer mechanism is dominant over the momentum transfer. This fact can be understood as follows: the electrohydrodynamic force can be written as $\rho_c\vec{E} = \vec{\nabla}p_E$, where $p_E = \epsilon_0 E^2/2$ is the electrostatic pressure; for a maximum electric field available in sprites of $\sim 5E_k$ (in streamer tips), we have $p_E \simeq 4\times10^{-6}$ Pa, which is significantly weaker than the local changes in pressure due to air heating, which are $\sim 10^{-3} - 10^{-2}$ Pa. Note that this analysis overestimates the effects of the electrohydrodynamic force because the residence time of a streamer head (of $\sim$1–10 μs), in a volume of space where the head passes through, is significantly shorter than the time scale for fast air heating (of $\sim\tau_p$). The inefficiency of momentum transfer by streamer discharges at sprite altitudes was also discussed by *Ebert et al.* [2006, Section 3.4]. To conclude, this analysis demonstrates that air heating or, more precisely, fast air heating is the physical mechanism responsible for infrasonic acoustic radiation from sprites.

Acknowledgments
This research was supported by NSF AGS-0734083 and AGS-1332199 grants to Penn State University. The authors gratefully acknowledge discussions with Jianqi Qin.

The Editor thanks two anonymous reviewers for their assistance in evaluating this paper.

References

Barrington-Leigh, C. P., V. P. Pasko, and U. S. Inan (2002), Exponential relaxation of optical emissions in sprites, *J. Geophys. Res.*, *107*(A5), SIA 6-1–SIA 6-10, doi:10.1029/2001JA900117.

Bastien, F. (1987), Acoustics and gas discharges: Applications to loudspeakers, *J. Phys. D: Appl. Phys.*, *20*(12), 1547–1557, doi:10.1088/0022-3727/20/12/001.

Bedard, A. J., W. A. Lyons, R. A. Armstrong, B. Hill, and S. Gallagher (1999), A search for low-frequency atmospheric acoustic waves associated with sprites, blue jets, elves, and storm electrical activity, *EOS Trans. AGU*, *80*(46), Fall Meet. Suppl., Abstract A51B–18.

Blackstock, D. T. (2000), *Fundamentals of Physical Acoustics*, 541 pp., John Wiley, New York.

Boeuf, J. P., Y. Lagmich, T. Unfer, T. Callegari, and L. C. Pitchford (2007), Electrohydrodynamic force in dielectric barrier discharge plasma actuators, *J. Phys. D: Appl. Phys.*, *40*(3), 652–662, doi:10.1088/0022-3727/40/3/S03.

Cummer, S. A., U. S. Inan, T. F. Bell, and C. P. Barrington-Leigh (1998), ELF radiation produced by electrical currents in sprites, *Geophys. Res. Lett.*, *25*(8), 1281–1284, doi:10.1029/98GL50937.

Cummer, S. A., N. C. Jaugey, J. B. Li, W. A. Lyons, T. E. Nelson, and E. A. Gerken (2006), Submillisecond imaging of sprite development and structure, *Geophys. Res. Lett.*, *33*, L04104, doi:10.1029/2005GL024969.

da Silva, C. L., and V. P. Pasko (2012), Simulation of leader speeds at gigantic jet altitudes, *Geophys. Res. Lett.*, *39*, L13805, doi:10.1029/2012GL052251.

da Silva, C. L., and V. P. Pasko (2013a), Dynamics of streamer-to-leader transition at reduced air densities and its implications for propagation of lightning leaders and gigantic jets, *J. Geophys. Res. Atmos.*, *118*, 13,561–13,590, doi:10.1002/2013JD020618.

da Silva, C. L., and V. P. Pasko (2013b), Vertical structuring of gigantic jets, *Geophys. Res. Lett.*, *40*, 3315–3319, doi:10.1002/grl.50596.

de Larquier, S. (2010), Finite-difference time-domain modeling of infrasound propagation in a realistic atmosphere, Master's thesis, Pennsylvania State Univ., University Park, Pa.

de Larquier, S., and V. P. Pasko (2010), Mechanism of inverted-chirp infrasonic radiation from sprites, *Geophys. Res. Lett.*, *37*, L24803, doi:10.1029/2010GL045304.

Ebert, U., C. Montijn, T. M. P. Briels, W. Hundsdorfer, B. Meulenbroek, A. Rocco, and E. M. van Veldhuizen (2006), The multiscale nature of streamers, *Plasma Sources Sci. Technol.*, *15*, 118–129, doi:10.1088/0963-0252/15/2/S14.

Farges, T., and E. Blanc (2010), Characteristics of infrasound from lightning and sprites near thunderstorm areas, *J. Geophys. Res.*, *115*, A00E31, doi:10.1029/2009JA014700.

Farges, T., E. Blanc, A. L. Pichon, T. Neubert, and T. H. Allin (2005), Identification of infrasound produced by sprites during the Sprite2003 campaign, *Geophys. Res. Lett.*, *32*, L01813, doi:10.1029/2004GL021212.

Few, A. A. (1986), Acoustic radiations from lightning, in *The Earth's Electrical Environment*, pp. 46–60, National Academy Press, Washington, D. C.

Gordillo-Vazquez, F. J. (2008), Air plasma kinetics under the influence of sprites, *J. Phys. D: Appl. Phys.*, *41*, 234016, doi:10.1088/0022-3727/41/23/234016.

Gordillo-Vazquez, F. J., and A. Luque (2010), Electrical conductivity in sprite streamer channels, *Geophys. Res. Lett.*, *37*, L16809, doi:10.1029/2010GL044349.

Hager, W. W., et al. (2012), Charge rearrangement by sprites over a north Texas mesoscale convective system, *J. Geophys. Res.*, *117*, D22101, doi:10.1029/2012JD018309.

Kanmae, T., H. C. Stenbaek-Nielsen, M. G. McHarg, and R. K. Haaland (2012), Diameter-speed relation of sprite streamers, *J. Phys. D: Appl. Phys.*, *45*, 275203, doi:10.1088/0022-3727/45/27/275203.

Kuo, C. L., et al. (2008), Radiative emission and energy deposition in transient luminous events, *J. Phys. D: Appl. Phys.*, *41*, 234014, doi:10.1088/0022-3727/41/23/234014.

Liszka, L. (2004), On the possible infrasound generation by sprites, *J. Low Freq. Noise Vib. Act. Control*, *23*(2), 85–93, doi:10.1260/0263092042869838.

Liu, N. (2010), Model of sprite luminous trail caused by increasing streamer current, *Geophys. Res. Lett.*, *37*, L04102, doi:10.1029/2009GL042214.

Liu, N. Y., V. P. Pasko, K. Adams, H. C. Stenbaek-Nielsen, and M. G. McHarg (2009), Comparison of acceleration, expansion, and brightness of sprite streamers obtained from modeling and high-speed video observations, *J. Geophys. Res.*, *114*, A00E03, doi:10.1029/2008JA013720.

Luque, A., and U. Ebert (2010), Sprites in varying air density: Charge conservation, glowing negative trails and changing velocity, *Geophys. Res. Lett.*, *37*, L06806, doi:10.1029/2009GL041982.

Pasko, V. P., and J. B. Snively (2007), Mechanism of infrasound radiation from sprites, *EOS Trans. AGU*, *88*(52), Fall Meet. Suppl., Abstract AE23A–0899.

Pasko, V. P., U. S. Inan, T. F. Bell, and S. C. Reising (1998), Mechanism of ELF radiation from sprites, *Geophys. Res. Lett.*, *25*(18), 3493–3496, doi:10.1029/98GL02631.

Popov, N. A. (2011), Fast gas heating in a nitrogen-oxygen discharge plasma: I. Kinetic mechanism, *J. Phys. D: Appl. Phys.*, *44*, 285201, doi:10.1088/0022-3727/44/28/285201.

Qin, J., S. Celestin, V. P. Pasko, S. A. Cummer, M. G. McHarg, and H. C. Stenbaek-Nielsen (2013), Mechanism of column and carrot sprites derived from optical and radio observations, *Geophys. Res. Lett.*, *40*, 4777–4782, doi:10.1002/GRL.50910.

Raizer, Y. P. (1991), *Gas Discharge Physics*, Springer, New York.

Roth, J. R. (2003), Aerodynamic flow acceleration using paraelectric and peristaltic electrohydrodynamic effects of a one atmosphere uniform glow discharge plasma, *Phys. Plasmas*, *10*(5,2), 2117–2126, doi:10.1063/1.1564823.

Sentman, D. D., E. M. Wescott, D. L. Osborne, D. L. Hampton, and M. J. Heavner (1995), Preliminary results from the Sprites94 aircraft campaign: 1. Red sprites, *Geophys. Res. Lett.*, *22*(10), 1205–1208, doi:10.1029/95GL00583.

Sentman, D. D., et al. (2003), Simultaneous observations of mesospheric gravity waves and sprites generated by a midwestern thunderstorm, *J. Atmos. Sol. Terr. Phys.*, *65*(5), 537–550, doi:10.1016/S1364-6826(02)00328-0.

Sentman, D. D., H. C. Stenbaek-Nielsen, M. G. McHarg, and J. S. Morrill (2008), Plasma chemistry of sprite streamers, *J. Geophys. Res.*, *113*, D11112, doi:10.1029/2007JD008941.

Stenbaek-Nielsen, H. C., and M. G. McHarg (2008), High time-resolution sprite imaging: Observations and implications, *J. Phys. D: Appl. Phys.*, *41*, 234009, doi:10.1088/0022-3727/41/23/234009.

Straumann, U. (2011), Mechanism of the tonal emission from ac high voltage overhead transmission lines, *J. Phys. D: Appl. Phys.*, *44*, 075501, doi:10.1088/0022-3727/44/7/075501.